3D Scan Registration using Curvelet Features

Siddhant Ahuja[1] and Steven L. Waslander[2]

University of Waterloo, Waterloo, ON, Canada, N2L 3G1

Abstract—Scan registration methods can often suffer from convergence and accuracy issues when the scan points are sparse or the environment violates the assumptions the methods are founded on. We propose an alternative approach to 3D scan registration using the curvelet transform that performs multi-resolution geometric analysis to obtain a set of coefficients indexed by scale (coarsest to finest), angle and spatial position. Features are detected in the curvelet domain to take advantage of the directional selectivity of the transform. A descriptor is computed for each feature by calculating the 3D spatial histogram of the image gradients, and nearest neighbor based matching is used to calculate the feature correspondences. Correspondence rejection using Random Sample Consensus identifies inliers, and a locally optimal Singular Value Decomposition-based estimation of the rigid-body transformation aligns the laser scans given the re-projected correspondences in the metric space. Experimental results on a publicly available dataset of planetary analogue facility demonstrates improved performance over existing methods.

I. INTRODUCTION

Sensors such as RGB-D cameras, LIDAR, Time of Flight (ToF), and stereo cameras provide information as point-sampled 3D surfaces, termed point-clouds. Overlapping scans share a common set of points that can be used for matching in order to estimate the relative rigid body transformation between scans (6-DOF rotation and translation). Separate views of the same environment can be accumulated into a global coordinate system which helps an intelligent mobile robot perform tasks in an unstructured environment. Finding accurate transformation parameters given a relatively large initial inter-scan transformation error, makes the registration problem especially hard.

Instead of working in the metric space, transform-based scan registration methods can often take advantage of the special properties of the transformations and improve the overall efficiency. Among various multi-scale transformations, curvelet transform is one of the many multi-resolution geometric analysis techniques that generates a sparse representation of the 3D laser scan and efficiently represents the underlying surface structure with high anisotropic elements (edges and singularities along curves) as a set of coefficients that capture details from coarse to fine levels. The curvelet transform has been widely used in the computer vision and image processing fields for image denoising, feature extraction, edge enhancement, and image fusion, among others.

In this work, we present a novel approach to scan registration using the *curvelet transform*. Instead of using an approximate sub-band of curvelet coefficients to solve the dimensionality problem, we instead find suitable features in the curvelet domain via difference of curvelets operator at multiple scales followed by extrema detection and filtering. Feature descriptors around the candidate keypoints are computed from 3D spatial histograms of image gradients and the correspondences are found using nearest neighbor matching. Feature correspondences are filtered using Random Sample Consensus (RANSAC) to reject outliers and the laser scans are aligned using Singular Value Decomposition (SVD) based estimation of rigid body transformation.

The rest of the paper is organized as follows: Section 2 provides the related work in the area of scan registration and a problem formulation is presented in Section 3. Details of the proposed method are given in Section 4. Quantitative and qualitative results for an indoor 3D laser scan dataset are provided in Section 5 with a discussion on suitability of the algorithm for mapping. Section 6 concludes the paper with directions for future work.

II. PREVIOUS WORK

One of the most popular scan registration methods-iterative closest point (ICP) [1]–[3] relies on point-to-point correspondences to estimate the relative transformation of scans by minimizing the Euclidean distance error metric. The original ICP algorithm assumes that there exists a correspondence between each point of the source and model datasets. This assumption is often violated with partially overlapping scans. Some modifications to the ICP algorithm have included the maximum error cutoff metric to account for false correspondences, and did not require every point to be matched. One of the key problems is that the sparsely sampled corresponding points in two different scans often do not correspond to the same point in the 3D environment, but ICP assumes that they do. In addition, the quality of the ICP solution depends heavily on the availability of good initial estimates of the transformation [1].

Many extensions to the original ICP have been proposed that transform the point clouds from metric space to feature space for fast correspondence based matching. They rely on finding unique features in the two scans, in order to improve the registration accuracy. Features based on color and intensity values [4], normals [5], [6], curvatures [7], integral volume descriptors [8], moment invariants [9], spherical harmonics [10], spin images [11], corners, lines and planes [12], [13], the scale-invariant feature transform (SIFT) [14], and combinations of the above [15] have all been suggested. However, all of these features are prone to measurement noise and cannot deal with varying sampling density within the point cloud. Locally

[1]PhD. Candidate, Mechanical and Mechatronics Engineering, University of Waterloo `s3ahuja at uwaterloo.ca`

[2]Assistant Professor, Mechanical and Mechatronics Engineering, University of Waterloo `stevenw at uwaterloo.ca`

planar surface structure was exploited by Segal et al. [16] for plane-to-plane correspondence search in generalized iterative closest point algorithm (GICP). The assumption of presence of planar structures restricts the applicability of the algorithm. Rusu et al. introduced the Sample Consensus-Initial Alignment (SAC-IA) algorithm [17] using 16-dimensional point feature histograms that describe the local surface structure. Experimental results showing the robustness of these features to outliers and invariance to pose, sampling density, and measurement noise are lacking in the literature. Various heuristics based on false correspondence rejection and re-weighting have tried to improve the robustness but the convergence is not guaranteed. In addition, these features require extensive computational steps and the resulting transformation is only an approximation due to the compact representation of a 3D surface (in metric space) as a feature point in feature space.

A relatively new approach to 3D point set registration algorithm is the normal distributions transform (NDT) that represents the underlying scene geometry as a Gaussian probability distribution [18], [19]. 3D-NDT partitions the space into disjoint volumetric cells called voxels and represents points within the voxels as a probability density function (PDF). One of the key benefits of this approach is that it forms piece-wise smooth spatial representations, however the division of points into voxels results in discontinuities in the cost function that make it susceptible to local minima [20]. Several variants based on multi-scale approaches have been proposed that minimize the discretization effects by calculating normal distributions from eight neighboring voxels and interpolating the weights [21], using K-means clustering [22], greedy clustering [23], and region-growing clustering with eigen-features [24].

Frequency-domain based approaches such as [25]–[27] decouple the problem of finding rotation and translation transformation parameters and attempt to find a suitable registration in the transformed domain. Phase correlation is typically employed for matching which is resilient to noise and occlusions, while fast Fourier transforms (FFT) used to compute cross-correlations makes this approach computationally efficient. However, the Fourier transform can only retrieve the global frequency content of the signal at the expense of time information and provides a dense representation of the underlying signal.

Another transformation found in the literature relies on finding a translation invariant Fourier domain transform on two Extended Gaussian Images (EGI) [28] of laser scans, however, this approach can only be applied to smooth surfaces and fails to match surfaces with constant EGI (such as a sphere). Censi et al. [29] proposed a new approach to scan matching that projects the two scans into the Hough/Radon domain [29] defined on the unit sphere. Similar to the work of Makaida et al. [28], a translation invariant spectrum is computed to find the rotation and 1D cross-correlations are used to find the translation. A major disadvantage shared by both EGI based approach and the ones based on transformation to Hough/Radon domain is the sensitivity of the algorithms to measurement noise and sampling density during the calculation of normals.

Unlike the shape-fixed rectangles in frequency domain of conventional FFT, multi-scale transforms such as discrete wavelet transform (DWT) use dilated shape varying rectangles to find directional elements such as edges and ridge features in the laser scans. However, many wavelet coefficients are needed to account for singularities along lines or curves. To overcome this problem, other directional wavelets such as wedgelets [30], beamlets [31], contourlets [32], surfacelets [33], etc. have been proposed, however the detected features are less prominent. In order to account for curve-singularities, curvelet transform has previously been proposed which generates an optimal sparse representation of the objects within the scan and employs angled polar wedges in the frequency domain to find directional features. Previously, Alam et al. applied curvelet transform for the problem of image fusion [34] where only an approximate sub-band of the coefficients was used for registration with an assumption of normal probability distribution of coefficients. This work has been inspired by the techniques used in the computer vision field for image fusion, and to the best knowledge of the authors, there has not been a detailed study of the application of curvelet transform for scan registration.

III. PROBLEM FORMULATION

Given two 3D point sets, model set $M = \{m_1, \cdots, m_{N_M}\}$ and data set $D = \{d_1, \cdots, d_{N_D}\}$ where $m_i, d_j \in \mathbb{R}^3$ for $i \in \{1, \cdots, N_M\}, j \in \{1, \cdots, N_D\}$, scan-to-scan registration algorithms obtain a 6-DOF relative alignment of the two scans that creates a single, globally consistent model of the environment by maximizing the similarity between scans after transformation. An estimate T of the true rigid body transformation $T^* = \{R, t\} \in \mathbb{SE}(3)$, with rotation $R = \{R_x, R_y, R_z\} \in \mathbb{SO}(3)$ and translation $t = \{t_x, t_y, t_z\} \in \mathbb{R}^3$ can be obtained from:

$$T^* = \underset{T \in \mathbb{SE}(3)}{\mathrm{argmax}}\, C(M, T(D)) \qquad (1)$$

where $C(M, T(D))$ is the similarity metric between the model set M and the transformed data set $T(D)$.

IV. PROPOSED METHOD

In order to incorporate curvelet transforms into the scan registration process, we define a similarity metric that is computed via a five-part algorithm as follows.

1) Range images R_M and $R_D \in I = \mathbb{R}_+^{X \times Y}$ of dimension $X \times Y$ are constructed from the spherical projections of the 3-D laser scans, M and D. Background regions surrounded by a connected border of foreground pixels are assigned an intensity value by employing a hole filling algorithm [35]. A Gaussian filter of size 3×3 with a standard deviation of 0.5 is used to smooth the range images and is followed by normalization of the range intensity values. Figure 1 shows the range image generated from the first 3D laser scan in the *a100* Mars

Dome dataset [36], with an angular resolution of 0.5 degrees in both x and y directions.
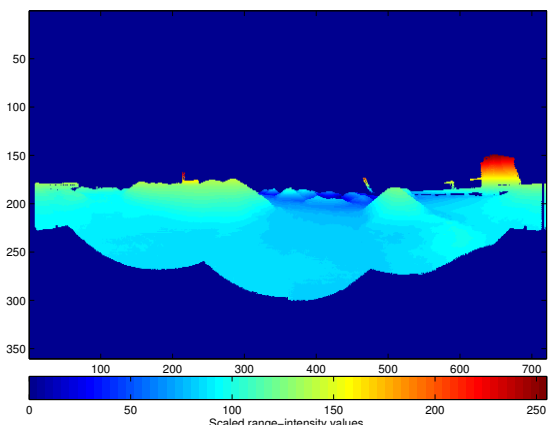
Fig. 1. Range image generated from the spherical projection of the first 3D laser scan in the *a100* Mars Dome dataset [36], with an angular resolution of 0.5 degrees in both x and y directions.

2) The discrete curvelet transform is then applied to each range image to obtain two sets of curvelet coefficients. The discrete curvelet transform is a linear digital transformation consisting of complex valued basis functions $\Psi_{j,l,k} : \mathbb{R}^2 \to \mathbb{C}$ parameterized in three spaces: scale $2^{-j} \in \mathbb{R}$, orientation $\theta_l[0, 2\pi) = 2\pi \cdot 2^{-\lfloor j/2 \rfloor} \cdot l$, where $l = 0, 1, \ldots 2\lfloor j/2 \rfloor - 1 \in \mathbb{Z}^1$, and scale dependent relative position $x_k^{(j,l)} = R_{\theta_l}^{-1}(k_1 2^{-j}, k_2 2^{\lfloor j/2 \rfloor}) \in I$, where $k = (k_1, k_2)$ indexes a standard translational grid that is adjusted to each scale value. The discrete curvelet transform of an $n \times m$ Cartesian array formed from the range image of size $X \times Y$ pixels is defined as the inner product between an element of the array $f(t_1, t_2) 0 \leq t_1 < n, 0 \leq t_2 < m$, and the curvelet basis function $\Psi_{j,l,k}$, given as [37]:

$$
\begin{aligned}
c(j, l, k) &= \langle f, \Psi_{j,l,k} \rangle \\
&= \sum_{0 \leq t_1 < n, 0 \leq t_2 < m} f[t_1, t_2] \Psi_{j,l,k}[t_1, t_2]
\end{aligned}
$$

where $\Psi_{j,l,k}$ is the basis function for the discrete version of the forward transform and $c(j, l, k)$ is the indexed curvelet coefficient. Curvelet transform implemented using second generation fast discrete curvelet transform (FDCT) via wrapping is available at http://www.curvelab.org. Figure 2 presents the log of the curvelet coefficients for the range image in Figure 1 for scales from the coarsest to level 4, and for angles from the 2nd coarsest to level 16. The center of the display shows the low frequency coefficients at the coarsest scale, with the Cartesian concentric coronae at the outer edges at various scale levels, showing coefficients at higher frequencies. Each corona contains four strips which are subdivided into angular panels [37].

---

[1]The notation $\lfloor x \rfloor$ denotes the floor of x, which truncates a positive real number to its integer component.
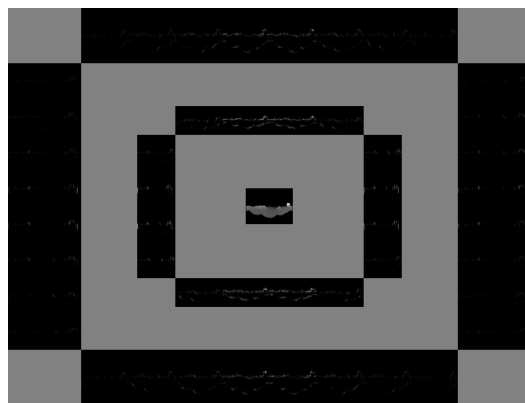
Fig. 2. Log of the curvelet coefficients for the range image in Figure 1 for $\lambda = 1 \ldots 4$ and $\phi = 2 \ldots 16$.

3) The Cartesian array formed from the range image can be reconstructed from the curvelet coefficients $c(j, l, k)$ by taking the inverse curvelet transform as [37]:

$$
I_c = \sum_{j,l,k} c(j, l, k) \tilde{\psi}_{j,l,k} \tag{2}
$$

where $\tilde{\Psi}_{j,l,k}$ is the basis function for inverse transform. Additionally, it is possible to invert each scale level individually, leading to scale dependent reconstructed images.

$$
I_c(j) = \sum_{l,k} c(j, l, k) \tilde{\psi}_{j,l,k} \tag{3}
$$

A novel differences of curvelets (DoC) image feature is introduced to identify stable locations that are invariant to scale. Contributions from individual sub-bands from two nearby scales is subtracted to produce a set of difference-of-curvelet images as follows:

$$
I_{DoC}(j) = I_c(j) - I_c(j-1) \tag{4}
$$

Similar to Scale Invariant Feature Transform (SIFT) [38], local maxima and minima over scale and space is used to find potential keypoints by comparing the pixel value at the current scale with its 8 connected neighbors, and 9 other pixels in both next and previous scales. The result is then thresholded to eliminate low-contrast keypoints, and keypoints lying close to the minimum cutoff range of the sensor, to obtain robust interest points (See Figure 3). A 16x16 neighborhood around the keypoint is used to obtain a 128 bin feature descriptor from the 3D spatial histogram of image gradients. This approach makes the algorithm robust against illumination changes.

4) A quick and efficient feature matching is performed using approximate nearest neighbor search in the feature space and feature correspondences are established between curvelet feature pairs. The nearest neighbor is defined as the feature with minimum Euclidean distance
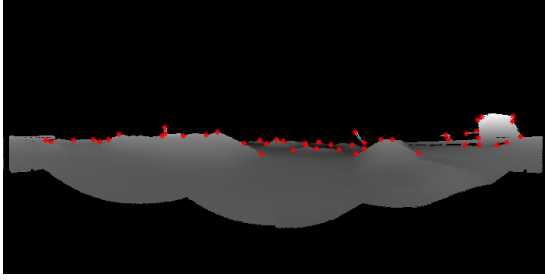
Fig. 3. Curvelet features (in red) from the range image in Figure 1.

to another feature in the feature space. Feature corre-
spondences are filtered using RANSAC to reject outliers.

5) Filtered corresponding curvelet feature pairs in the met-
ric space are used to estimate the rigid body transfor-
mation by employing SVD.

V. EXPERIMENTAL RESULTS

The proposed approach is evaluated using a planetary ana-
logue indoor dataset(the a100_dome) [36] consisting of 95
scans obtained by vertically scanning SICK LMS291-S05 laser
rangefinder with a vertical resolution of 0.5 degrees. The scans
were taken at the University of Toronto Institute for Aerospace
Studies (UTIAS) rover test facility at Toronto, Ontario. The
environment within the dome emulates unstructured Mars-like
terrain with sand, gravel, and hills. Registering scans from an
emulated Mars terrain is quite challenging as some laser scans
demonstrate low degree of overlap and lack sufficient features
to match the scans with each other, even with full 360° x
180° scans of the terrain (see Figure 4) . The poor structure
of the Mars like terrain coupled with the shallow grazing
angle results in a variable resolution, occluded, sparse range
data that is hard to register without some a-priori knowledge
of the environment. Ground truth data is provided from four
retroreflective markers.

The algorithms used for comparison are ICP, G-ICP, NDT,
SAC-IA, and Harris-3D with reference implementations pro-
vided in the point-cloud library (PCL) [39]. The ICP, G-
ICP and SAC-IA algorithms are implemented with maximum
correspondence distance set to 10m, and the NDT algorithm is
implemented with Newton line search maximum step length of
0.1, and voxel grid resolution of 2m. Surface normals for the
SAC-IA and Harris-3D algorithms are computed with a radius
search parameter of 0.5 m and normals are flipped towards
the sensor viewpoint. Harris-3D features are computed with
a threshold parameter set to 1e-5 and 33-dimensional FPFH
descriptors in both the Harris-3D and SAC-IA algorithms
are computed with the radius search set to 5 times the
radius for calculation of surface normals. RANSAC based
correspondence rejection and initial alignment computation
is performed for Harris-3D algorithm similar to steps 4-5 in
Section IV.

For all algorithms, the maximum iterations was set to 500
and the optimization was terminated when the norm of the

(a)

(b)

(c)
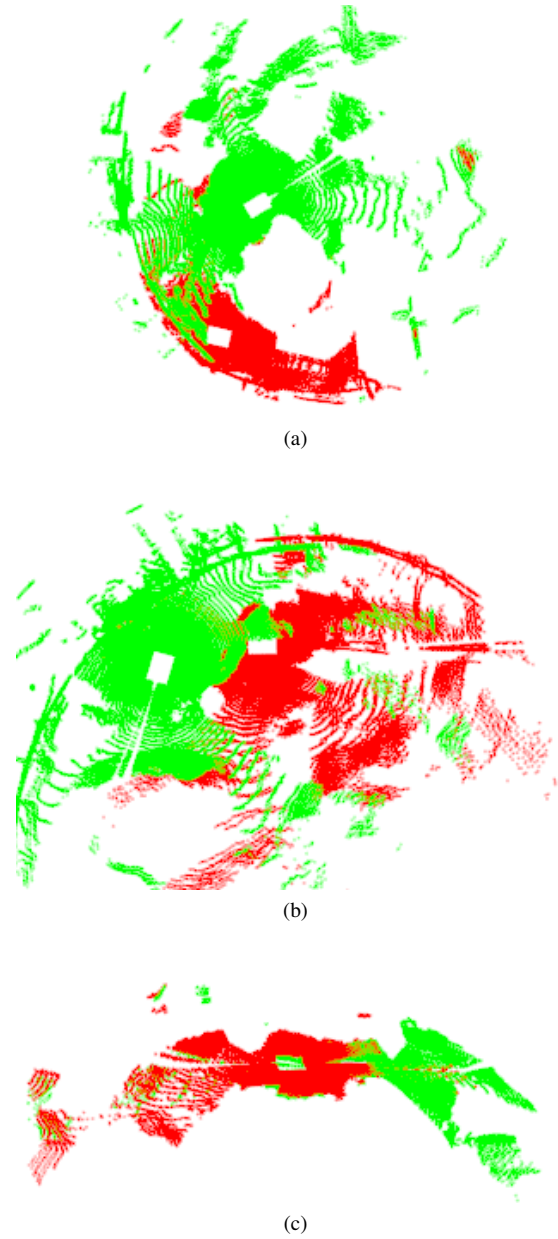
Fig. 4. Ground-truth-aligned pointclouds from *a100* Mars Dome dataset [36]
demonstrating low degree of overlap in (a-b) and lack of sufficient features
for scan registration (a-c). (a) Scans 10 and 11, (b) Scans 20 and 21, and (c)
Scans 60 and 61.

gradient or the norm of the step size falls below 10^{-6}. Pair-
wise scan registration was performed using every 10th scan
with initial conditions set to zero. The absolute error in rotation
and translation is compared with the ground truth measure-
ments. Figure 5 shows the empirical distribution function plots
for absolute translational and rotational errors. Assuming that
the error samples are independent and identically-distributed
random variables, the asymptotic behavior of the empirical
measure of the error samples can be determined using the
empirical cumulative distribution function [40]. It is defined
as the proportion of error samples less than or equal to a given
error metric, converging with a probability of one.

	Absolute Translation Error (m)		Absolute Rotation Error (rad)	
	Median	MAD	Median	MAD
ICP	2.9699	1.2405	0.4419	0.3339
G-ICP	2.4635	1.1339	0.3424	0.2346
NDT	2.6705	0.9397	0.5465	0.4571
SAC-IA	1.2903	0.8528	0.1304	0.0681
Harris-3D	0.3615	0.2220	0.0358	0.0197
Proposed Method	**0.1936**	**0.1038**	**0.0274**	**0.0224**

The error distributions from Figure 5 demonstrate that curvelet transform based scan registration demonstrates a faster convergence to a probability of one, thereby achieving a higher percentage of registered scans with lowest error metric when compared with other methods. The median and median absolute deviations (MAD) for absolute errors in translation and rotation given in Table V.

The large translational and rotational error in NDT can be attributed to the poor convergence properties of NDT. The quality of alignment is directly dependent on the degree of scan overlap, point selection strategy and accurate correspondences. Both ICP and G-ICP algorithms show high translational and rotational errors due to the lack of feature-rich regions in the scans and absence of planar structures. SAC-IA algorithm demonstrates a lower error as compared with ICP, G-ICP and NDT algorithms as only persistent features are used for matching, however since it requires the computation of surface normals, it suffers from the problem of finding the correct radius size, given the resolution of the scan. Harris-3D algorithm finds corner points in the scan from the gradients of surface normals. In addition to the radius problem described before, Harris3D often considers points lying in the depth-discontinuous regions of the scan as corner points. Due to poor feature locations and inaccurate feature correspondences, Harris3D fails in scans that lack sufficient number of corner points. Compared with other algorithms, curvelet transform based scan registration demonstrates low translational and rotational error.

Figure 6 displays the close-up views of the fifth registered scan-pair using ICP, G-ICP, NDT, SAC-IA, Harris-3D and curvelet methods. Visually, the resulting aggregated registered scans using Harris-3D and curvelet algorithms demonstrate better alignment as compared with other algorithms. However, for this scan pair, curvelet based registration results in lower absolute translational and rotational error.

VI. CONCLUSIONS AND FUTURE WORK

This work presents a curvelet transform based method for improving the convergence properties of standard registration algorithms. Instead of using an approximate sub-band of curvelet coefficients to solve the dimensionality problem, we instead find suitable features in the curvelet domain via

(a)

(b)
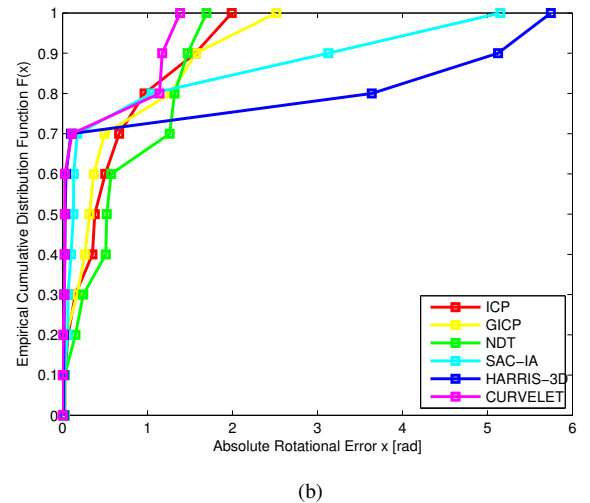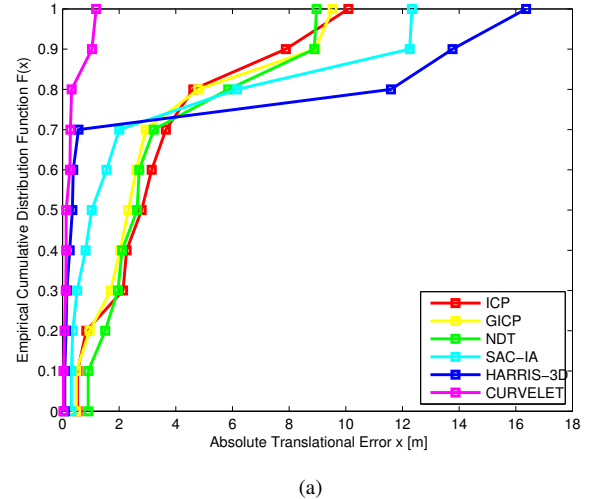
Fig. 5. Empirical cumulative distribution function plots for errors in transformation parameters for *a100* Mars Dome dataset [36], (a) Absolute translational error (m). (b) Absolute rotational error (rad).

difference of curve lets operator at multiple scales followed by extrema detection and filtering. Feature descriptors around the candidate keypoints are computed from 3D spatial histograms of image gradients and the correspondences are found using nearest neighbor matching. Feature correspondences are filtered using Random Sample Consensus (RANSAC) to reject outliers and the laser scans are aligned using Singular Value Decomposition (SVD) based estimation of rigid body transformation. Experimental results on a publicly available dataset of planetary analogue facility demonstrates improved performance over existing methods.

REFERENCES

[1] P. J. Besl and N. D. McKay, "A method for registration of 3-d shapes," *IEEE Transactions on Pattern Analysis and Machine Intelligence*, vol. 14, no. 2, pp. 239–256, February 1992.

[2] Y. Chen and G. Medioni, "Object modeling by registration of multiple range images," in *Proceedings of IEEE International Conference on*

Robotics and Automation (ICRA), vol. 3, Sacramento, CA, USA, April 1991, pp. 2724–2729.

[3] Z. Zhang, "Iterative point matching for registration of free-form curves and surfaces," *International Journal of Computer Vision*, vol. 13, no. 2, pp. 119–152, October 1994.

[4] G. Godin, M. Rioux, and R. Baribeau, "Three-dimensional registration using range and intensity information," in *Proceedings of the SPIE: Videometrics III*, vol. 2350. Boston, Massachusetts, USA: SPIE, November 1994, pp. 279–290.

[5] Y. Ioanou, B. Taati, R. Harrap, and M. Greenspan, "Difference of normals as a multi-scale operator in unorganized point clouds," in *Second International Conference on 3D Imaging, Modeling, Processing, Visualization and Transmission (3DIMPVT)*, ETH Zürich, Switzerland, October 2012, pp. 501–508.

[6] M. Alexa and A. Adamson, "On normals and projection operators for surfaces defined by point sets," in *Eurographics Symposium on Point-Based Graphics*, ETH Zürich, Switzerland, June 2004, pp. 149–155.

[7] C. S. Chua and R. Jarvis, "3d free-form surface registration and object recognition," *International Journal of Computer Vision*, vol. 17, no. 1, pp. 77–99, January 1996.

[8] N. Gelfand, N. J. Mitra, L. J. Guibas, and H. Pottmann, "Robust global registration," in *Proceedings of the third Eurographics symposium on Geometry processing*, ser. SGP '05. Aire-la-Ville, Switzerland, Switzerland: Eurographics Association, July 2005.

[9] F. A. Sadjadi and E. L. Hall, "Three-dimensional moment invariants," *IEEE Transactions on Pattern Analysis and Machine Intelligence*, vol. PAMI-2, no. 2, pp. 127–136, March 1980.

[10] G. Burel and H. Henocq, "Three-dimensional invariants and their application to object recognition," *Signal Processing*, vol. 45, no. 1, pp. 1–22, July 1995.

[11] A. Johnson and M. Hebert, "Recognizing objects by matching oriented points," in *Proceedings of IEEE Computer Society Conference on Computer Vision and Pattern Recognition*, San Juan, Puerto Rico, June 1997, pp. 684–689.

[12] A. Censi, L. Iocchi, and G. Grisetti, "Scan matching in the hough domain," in *Proceedings of the IEEE International Conference on Robotics and Automation (ICRA)*, Barcelona, Spain, April 2005, pp. 2739–2744.

[13] I. Sipiran and B. Bustos, "A robust 3d interest points detector based on harris operator," in *Proceedings of the 3rd Eurographics conference on 3D Object Retrieval*, ser. EG 3DOR'10. Aire-la-Ville, Switzerland, Switzerland: Eurographics Association, May 2010, pp. 7–14.

[14] P. Henry, M. Krainin, E. Herbst, X. Ren, and D. Fox, "Rgb-d mapping: Using kinect-style depth cameras for dense 3d modeling of indoor environments," *International Journal of Robotics Research*, vol. 31, no. 5, pp. 647–663, April 2012.

[15] G. Sharp, S.-W. Lee, and D. Wehe, "Icp registration using invariant features," *IEEE Transactions on Pattern Analysis and Machine Intelligence*, vol. 24, no. 1, pp. 90–102, January 2002.

[16] A. Segal, D. Haehnel, and S. Thrun, "Generalized-icp," in *Proceedings of Robotics: Science and Systems (RSS)*, vol. 25, Seattle, WA, USA, June 2009, pp. 26–27.

[17] R. B. Rusu, N. Blodow, Z. C. Marton, and M. Beetz, "Aligning point cloud views using persistent feature histograms," in *IEEE/RSJ International Conference on Intelligent Robots and Systems (IROS)*, Nice, France, September 2008, pp. 3384–3391.

[18] P. Biber and W. Strasser, "The normal distributions transform: a new approach to laser scan matching," in *Proceedings of IEEE/RSJ International Conference on Intelligent Robots and Systems (IROS)*, vol. 3, Las Vegas, Nevada, USA, October 2003, pp. 2743–2748.

[19] M. Magnusson, A. Lilienthal, and T. Duckett, "Scan registration for autonomous mining vehicles using 3d-ndt," *Journal of Field Robotics*, vol. 24, no. 10, pp. 803–827, October 2007.

[20] M. Magnusson, "The three-dimensional normal-distributions transform – an efficient representation for registration, surface analysis, and loop detection," Ph.D. dissertation, Orebro University, December 2009.

[21] M. Magnusson, A. Nuchter, C. Lorken, A. Lilienthal, and J. Hertzberg, "Evaluation of 3d registration reliability and speed - a comparison of icp and ndt," in *IEEE International Conference on Robotics and Automation (ICRA)*, Kobe, Japan, May 2009, pp. 3907–3912.

[22] A. Das and S. Waslander, "Scan registration with multi-scale k-means normal distributions transform," in *IEEE/RSJ International Conference on Intelligent Robots and Systems (IROS)*, Vilamoura, Algarve, Portugal, October 2012, pp. 2705–2710.

[23] A. Das, J. Servos, and S. Waslander, "3d scan registration using the normal distributions transform with ground segmentation and point cloud clustering," in *Proceedings of IEEE International Conference on Robotics and Automation (ICRA)*, Karlsruhe, Germany, May 2013, pp. 2207–2212.

[24] S. Ahuja and S. L. Waslander, "Scan registration using the normal distributions transform with region growing clustering for point-sampled 3d surfaces," in *AIAA Guidance, Navigation, and Control Conference*, National Harbor, MD, United States, January 2014.

[25] H. Bulow and A. Birk, "Spectral 6dof registration of noisy 3d range data with partial overlap," *IEEE Transactions on Pattern Analysis and Machine Intelligence*, vol. 35, no. 4, pp. 954–969, 2013.

[26] L. Lucchese, G. Doretto, and G. Cortelazzo, "A frequency domain technique for range data registration," *IEEE Transactions on Pattern Analysis and Machine Intelligence*, vol. 24, no. 11, pp. 1468–1484, 2002.

[27] Y. Keller, Y. Shkolnisky, and A. Averbuch, "Volume registration using the 3-d pseudopolar fourier transform," *IEEE Transactions on Signal Processing*, vol. 54, no. 11, pp. 4323–4331, 2006.

[28] A. Makadia, A. Patterson, IV, and K. Daniilidis, "Fully automatic registration of 3d point clouds," in *Proceedings of the IEEE Computer Society Conference on Computer Vision and Pattern Registration (CVPR)*, 2006, pp. 1297–1304.

[29] A. Censi and S. Carpin, "HSM3D: Feature-less global 6DOF scan-matching in the Hough/Radon domain," in *Proceedings of the IEEE International Conference on Robotics and Automation (ICRA)*, May 2009.

[30] D. L. Donoho, "Wedgelets: nearly-minimax estimation of edges," *The Annals of Statistics*, vol. 27, no. 3, pp. 859–897, June 1999.

[31] D. Donoho and X. Huo, *Beamlets and Multiscale Image Analysis*, ser. Lecture Notes in Computational Science and Engineering, T. Barth, T. Chan, and R. Haimes, Eds. Springer Berlin Heidelberg, 2002, vol. 20.

[32] M. Do and M. Vetterli, "The contourlet transform: an efficient directional multiresolution image representation," *IEEE Transactions on Image Processing*, vol. 14, no. 12, pp. 2091–2106, 2005.

[33] Y. Lu and M. Do, "Multidimensional directional filter banks and surfacelets," *IEEE Transactions on Image Processing*, vol. 16, no. 4, pp. 918–931, 2007.

[34] M. Alam, T. Howlader, and S. Rahman, "Entropy-based image registration method using the curvelet transform," *Signal, Image and Video Processing*, pp. 1–15, 2012.

[35] P. Soille, *Morphological Image Analysis: Principles and Applications*, 2nd ed. Secaucus, NJ, USA: Springer-Verlag New York, Inc., 2003.

[36] C. H. Tong and T. Barfoot, "A self-calibrating 3d ground-truth localization system using retroreflective landmarks," in *IEEE International Conference on Robotics and Automation (ICRA)*, Shanghai, China, May 2011, pp. 3601–3606.

[37] E. Candès, L. Demanet, D. Donoho, and L. Ying, "Fast discrete curvelet transforms," *Multiscale Modeling and Simulation*, vol. 5, no. 3, pp. 861–899, 2006.

[38] D. Lowe, "Distinctive image features from scale-invariant keypoints," *International Journal of Computer Vision*, vol. 60, no. 2, pp. 91–110, 2004.

[39] R. Rusu and S. Cousins, "3d is here: Point cloud library (pcl)," in *IEEE International Conference on Robotics and Automation (ICRA)*, Shanghai, China, May 2011, pp. 1–4.

[40] H. G. Tucker, "A generalization of the glivenko-cantelli theorem," *The Annals of Mathematical Statistics*, vol. 30, no. 3, pp. 828–830, 09 1959.
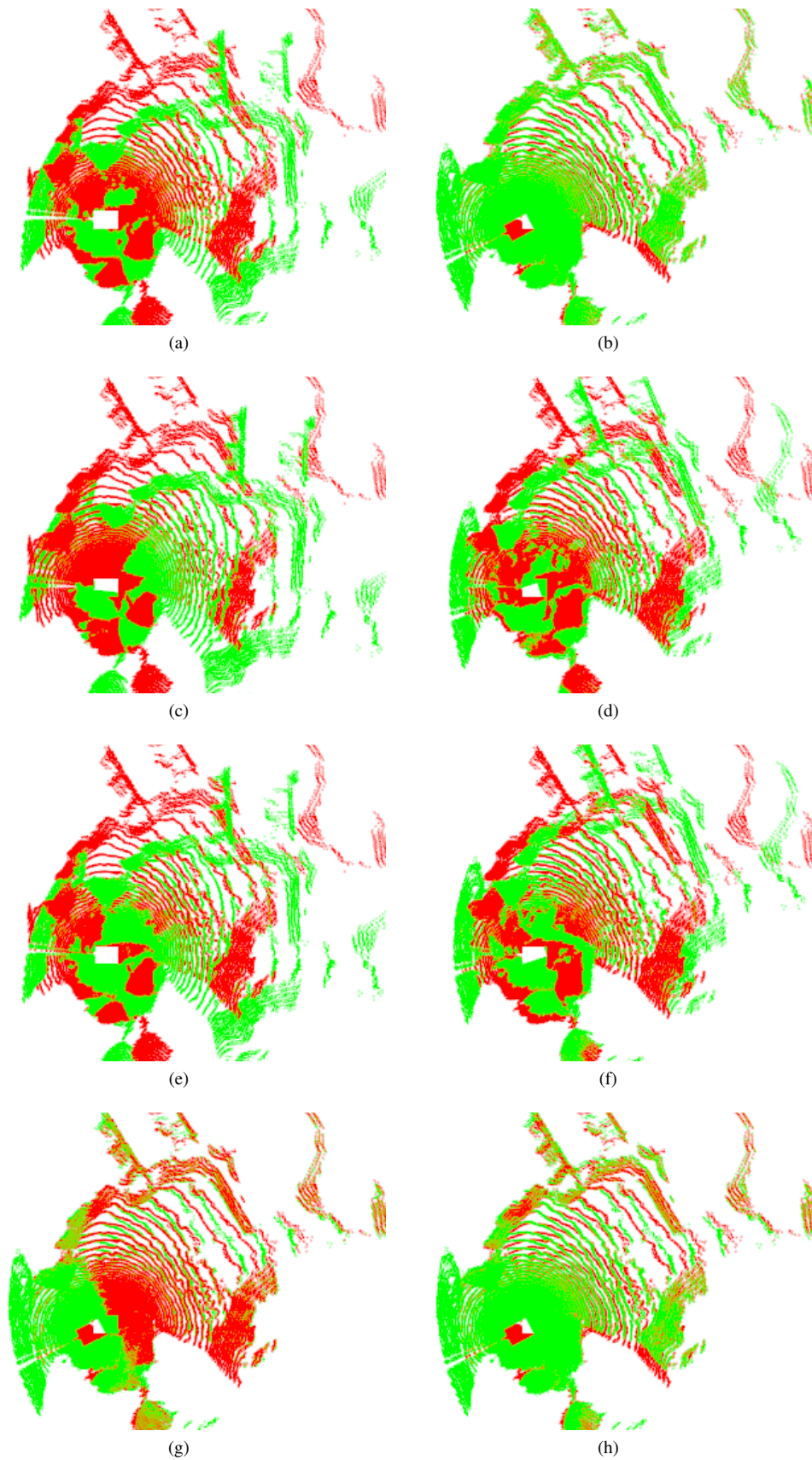
Fig. 6. Registered laser scans 40 (red) and 41 (green) from *a100* Mars Dome dataset [36], (a) No alignment (b) Ground Truth (c) ICP (d) GICP (e) NDT (f) SAC-IA (g) Harris-3D (h) Proposed Method. (best viewed in colour)